The American Journal of Pathology, Vol. 173, No. 4, October 2008

DOI: 10.2353/ajpath.2008.071183

Tumorigenesis and Neoplastic Progression

Hypoxia Inducible Factor-1α Inactivation Unveils a Link between Tumor Cell Metabolism and Hypoxia-Induced Cell Death

Elena Favaro,* Giorgia Nardo,* Luca Persano,* Massimo Masiero,* Lidia Moserle,* Rita Zamarchi,† Elisabetta Rossi,* Giovanni Esposito,† Mario Plebani,‡ Ulrike Sattler,§ Thomas Mann,§ Wolfgang Mueller-Klieser,§ Vincenzo Ciminale,* Alberto Amadori,*† and Stefano Indraccolo†

From the Department of Oncology and Surgical Sciences, Oncology Section, University of Padova, Padova, Italy; Istituto Oncologico Veneto-Instituto di Ricovero e Cura Scientifico,† Padova, Italy; Department of Laboratory Medicine, Medical and Surgical Sciences,‡ University of Padova, Padova, Italy; and Institute of Physiology and Pathophysiology,§ University of Mainz, Mainz, Germany*

Hypoxia and the acquisition of a glycolytic phenotype are intrinsic features of the tumor microenvironment. The hypoxia inducible factor-1α (HIF-1α) pathway is activated under hypoxic conditions and orchestrates a complex transcriptional program that enhances cell survival. Although the consequences of HIF-1α inactivation in cancer cells have been widely investigated, only a few studies have addressed the role of HIF-1α in the survival of cancer cells endowed with different glycolytic capacities. In this study, we investigated this aspect in ovarian cancer cells. Hypoxia-induced toxicity was increased in highly glycolytic cells compared with poorly glycolytic cells; it was also associated with a sharp decrease in intracellular ATP levels and was prevented by glucose supplementation. Stable HIF-1α silencing enhanced hypoxia-induced cell death *in vitro* due to a lack of cell cycle arrest. Tumors bearing attenuated HIF-1α levels had similar growth rates and vascularization as did controls, but tumors showed higher proliferation levels and increased necrosis. Moreover, tumors formed by HIF-1α deficient cells had higher levels of lactate and lower ATP concentrations than controls as shown by metabolic imaging. The findings that such metabolic properties can affect the survival of cancer cells under hypoxic conditions and that these properties contribute to the determination of the consequences of HIF-1α inactivation could have important implications on the understanding of the effects of anti-angiogenic and HIF-1α-targeting drugs in cancer. *(Am J Pathol 2008, 173:1186–1201; DOI: 10.2353/ajpath.2008.071183)*

Hypoxia, caused by increased metabolic activity and rapid cell proliferation impairing the vascular supply of oxygen and nutrients, is a hallmark of tumors (reviewed in:[1]). Moreover, it is now recognized that hypoxia can be modulated by novel therapies targeting tumor angiogenesis.[2–4] Anti-angiogenic therapy is believed to reduce blood supply, thus increasing hypoxia in the tumor microenvironment and leading to tumor starvation or death.[5]

Many cellular responses to hypoxia are regulated by the transcriptional factor hypoxia-inducible factor-1 (HIF-1);[6] HIF-1α is the regulatory subunit of HIF-1. Despite many studies (reviewed in:[7]), the role of HIF-1α in the regulation of hypoxic cell death remains controversial. In fact, although HIF-1α *trans*-activates genes that either increase angiogenesis or allow metabolic adaptation to hypoxic environment and are thus key to cell survival, this transcriptional factor has also been shown to play an active role in promoting apoptosis, through induction or stabilization of several pro-apoptotic factors, including P53, BNIP3, and BNIP3L (reviewed in:[8]).

The notion that early carcinogenesis occurs in a hypoxic microenvironment has suggested that the transformed cells rely on glycolysis for energy production.[9] This metabolic adaptation appears to confer a survival

Supported in part by grants from AIRC and FIRC; Ministry of University and Research, 60% and PRIN; Ministry of Health, Oncology Program 2006; Banco Popolare di Verona; and grants from the Mainzer Forschungsfoerderungsprogramm MAIFOR (#8277000).

Accepted for publication July 15, 2008.

Supplemental material for this article can be found on http://ajp.amjpathol.org.

Address reprint requests to Stefano Indraccolo, M.D., Istituto Oncologico Veneto - IRCCS, via Gattamelata, 64 - 35128 Padua – Italy. E-mail: stefano.indraccolo@unipd.it.

advantage, and it is commonly observed in most tumors even when they eventually become vascularized, a phenomenon termed the Warburg effect.[10] Because glycolysis produces energy (ATP) far less efficiently than oxidative phosphorylation, tumor cells have higher rates of glucose consumption than normal cells, which is further increased under hypoxic conditions.[9] Notably, although HIF-1α accumulation can promote glycolysis under hypoxic conditions, the Warburg effect implies that other molecular pathways contribute to determine the glycolytic phenotype of cancer cells (reviewed in:[9]). Interestingly, the intensity of the glycolytic phenotype can vary among tumors, as also reflected by different patterns of ^{18}F-fluoro-deoxyglucose uptake in patients undergoing positron emission tomography.[11]

Although one may expect that highly glycolytic tumor cells may have adapted to survive under hypoxic conditions, previous studies on the response of tumor cells to hypoxia have not looked into this question in detail.[12–19] Similarly, the contribution of HIF-1α to survival or death of cells with different metabolic properties remains unclear. These are relevant issues, because intrinsic or acquired sensitivity of tumor cells to hypoxia-induced cell death could reasonably play a role in determining the outcome of treatments with angiogenesis inhibitors.

In this study, we measured the levels of hypoxia-induced cell death in ovarian cancer cell lines and showed that their sensitivity to hypoxia-induced cell death *in vitro* directly correlated with their metabolic properties. Cancer cells resisted adverse effects of hypoxia until ATP levels were depleted and eventually died because of energy deprivation; this phenomenon was dependent on the intrinsic variations in the metabolic profile, resulting in a different glucose consumption rate of the cell lines analyzed. Importantly, HIF-1α attenuation enhanced cell proliferation and energy demand under hypoxic conditions, thus leading to early exhaustion of ATP and increased cell death.

Materials and Methods

Cell Culture

The ovarian cancer cell line IGROV-1 was purchased from ATCC (Manassas, VA); OC316 cells were kindly provided by S. Ferrini (Istituto Nazionale per la Ricerca sul Cancro, Genoa, Italy).

The primary ovarian cancer cell lines PDOVCA#2 and #4 were derived from the ascitic component of xenograft tumors grown i.p. in severe combined immunodeficiency (SCID) mice injected with malignant cells from ovarian cancer patients. Informed consent was obtained from the patients. Primary tumor cells grow *in vitro* only for a limited time (range, 2 to 4 weeks) and are routinely maintained as serial xenotransplants in mice as described elsewhere.[20]

Tumor cells were grown in RPMI 1640 medium (Euroclone, Pero, Italy) supplemented with 10% fetal calf serum (Life Technologies, Gaithersburg, MD), 10 mmol/L HEPES (Cambrex Bioscience, Verviers, Belgium), 2 mmol/L L-glutamine, and 1% antibiotics-antimycotic mix (Gibco-BRL, Grand Island, NY). The cultures were routinely maintained at 37°C in a humidified 5% CO_2/95% air atmosphere.

Hypoxic treatment of cells was achieved by incubating cells in a PROOX model 110 chamber (Biospherix, Redfield, NY). During incubation, a humidified environment at 37°C, 5% CO_2, and 0.1 to 0.3% O_2 was maintained. To determine the response of cancer cells to different hypoxia levels, percentages of O_2 ranging from 0.1% to 5% were used. The hypoxia-simulating drug cobalt chloride ($CoCl_2$; Sigma, St. Louis, MO) was used at a concentration of 100 μmol/L. In a set of experiments, taxol (Mayne Pharma, Napoli, Italy) was added to OC316 or IGROV-1 cells at 100 μg/ml for 48 hours as apoptosis-inducing drug.

Annexin V Apoptosis Assay

Cells were incubated with Annexin V-fluorescein isothiocyanate in HEPES buffer containing propidium iodide (PI), using the Annexin-V Fluos Staining Kit (Roche Diagnostics, Mannheim, Germany). Labeled cells were analyzed on an EPICS-XL cytofluorimeter using Expo32 software (Beckman Coulter, Fullerton, CA).

Glucose and Lactate Measurements

In a set of experiments, IGROV-1, OC316, PDOVCA#2, and PDOVCA#4 cells were exposed to normoxia or hypoxia for 24 to 48 hours. The glucose and lactate concentrations in the supernatants were determined by colorimetric methods on an automatic analyzer (Dimension RxL, Dade Behring, Milan, Italy). Values were normalized to cell numbers at the end of the incubation period. To measure the kinetics of lactate production, OC316 and IGROV-1 cells were seeded at 1×10^4 cells/cm^2 in six-well flat-bottom plates (Greiner Bio-One, Frickenhausen, Germany) in complete RPMI medium. After 2 days, the medium was changed and medium supernatant samples were taken at indicated times. Deproteinized medium supernatants were analyzed with a commercial photometric assay kit (r-biopharm, Darmstadt, Germany) in triplicates according to the manufacturer's instructions. Lactate concentrations were normalized to cell numbers, which were assessed by an automatic cell counter (CASY Technology, Reutlingen, Germany).

Measurement of ATP Levels

IGROV-1 and OC316 cells and their derivatives were plated in triplicate in 96-well plates at different densities (range: 1×10^4 to 2.5×10^4 cells/well) and subsequently exposed to normoxia or hypoxia for 48 hours. ATP levels were determined by the ViaLight HS Kit (Cambrex Bioscience) according to manufacturer's instructions, and normalized to the protein content of the lysates. In a set of experiments, to measure the ATP consumption rate, 1.0×10^5 cells were incubated in D5030 medium (Sigma) supplemented with 25 mmol/L HEPES without glucose

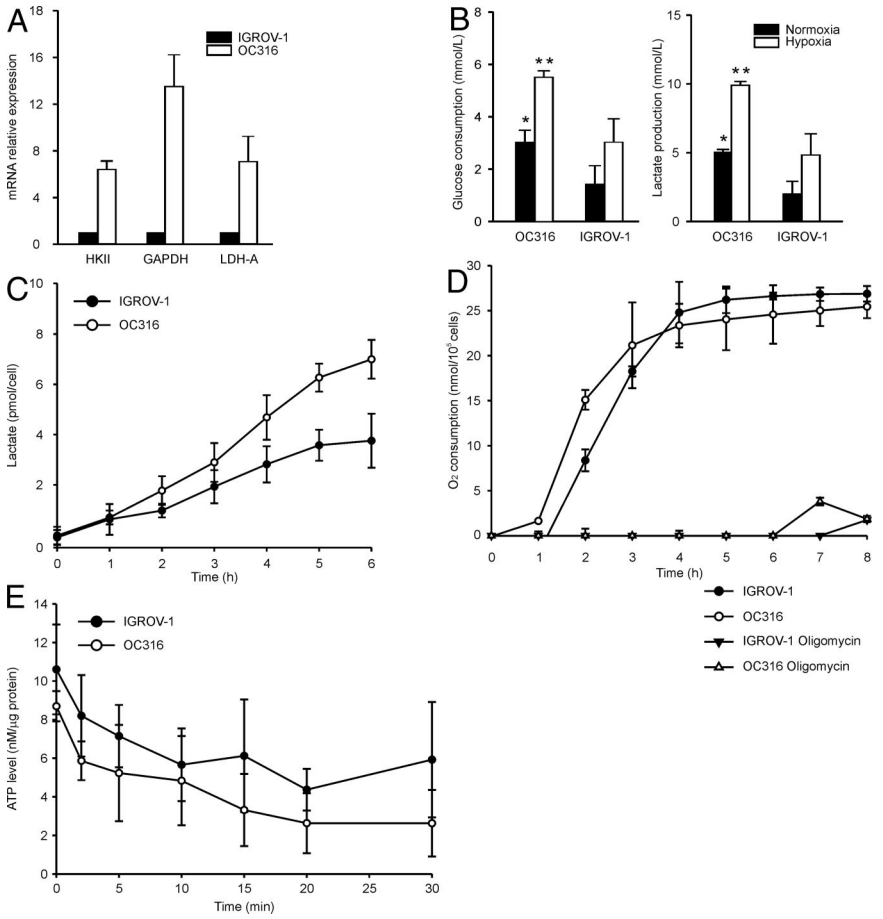

Figure 1. Identification of ovarian cancer cells with different metabolic properties. **A:** Expression of genes involved in glycolysis (HKII, GAPDH, and LDH-A) by quantitative PCR analysis in ovarian cancer cells. Expression of each gene was normalized to the β2-microglobulin transcript, used as housekeeping gene. The expression levels in IGROV-1 cells were then set at 1 and relative expression levels were calculated. Mean ± SD of three experiments is shown. **B:** Measurement of glucose consumption (left panel) and lactate production (right panel). Cells were plated in P6 wells at 1.5×10^5 cells/well, incubated for 24 hours *in vitro* under either normoxic or hypoxic conditions and metabolic parameters quantified by an automatic analyzer. Mean ± SD of four experiments is shown, with statistically significant differences between OC316 and IGROV-1 cells under normoxic (*) or hypoxic (**) conditions ($P < 0.05$). **C:** Kinetics of lactate production. Each sample was analyzed in triplicate and mean ± SD of three independent experiments is shown. After 6 hours, OC316 and IGROV-1 cells showed a lactate production of 7.02 pmol/cell and 3.85 pmol/cell, respectively (mean values). **D:** Measurement of oxygen consumption by OC316 and IGROV-1 cells. Values reported in the *y* axis represent the nmoles of O_2 consumed per 100,000 cells calculated as described in the Materials and Methods. Cells were cultured at 0.3×10^6 cells/well in OBS wells (Becton Dickinson) in D5030 medium, with or without oligomycin (0.2 μg/ml), as detailed in the Materials and Methods. Each sample was analyzed in triplicate and mean values ± SD of four independent experiments are shown. **E:** Measurement of the rates of ATP decay following substrate deprivation in OC316 and IGROV-1 cells. The ATP content was determined and normalized to the protein content of the lysates. Mean ± SD of three independent experiments is shown.

and cells were either immediately lysed or maintained in normoxic conditions followed by cell lysis and measurement of ATP levels at serial time points. The ATP consumption rate was expressed as [ATP ($t_{0\ minutes}$) − ATP ($t_{2\ minutes}$)]/2 minutes. Cell viability was assessed by Annexin V labeling after 30 minutes incubation in D5030 medium and it was similar in OC316 and IGROV-1 cells, ranging between 78.2% and 81.7%. To measure ATP consumption rates in transduced cells, OC316 ΔHIF-1α, and control cells were incubated in complete RPMI medium at 37°C, 5% CO_2, either under normoxic or hypoxic conditions. After 16 hours, RPMI medium was replaced with D5030 medium supplemented with 25 mmol/L HEPES and without glucose and cells were either immediately lysed or maintained in normoxic or hypoxic conditions for further 30 minutes followed by cell lysis and measurement of ATP levels.

Detection of Oxygen Consumption

Oxygen consumption by IGROV-1 and OC316 cells was measured using the BD Oxygen Biosensor System (BD Biosciences, Bedford, MA): 0.3×10^6 cells/well were plated in triplicate in 200 μl of D5030 medium supplemented with 10% fetal calf serum, 25 mmol/L HEPES, 2 mmol/L L-glutamine, 1 mmol/L Na-pyruvate, and 2 g/L glucose in a 96-well plate embedded with an oxygen-sensitive flurochrome. The plates were sealed to prevent oxygen uptake from the environment. The intensity of emitted fluorescence is directly correlated to the oxygen concentration in the well, and it was measured at different time points in a fluorescence plate reader at 485 nm excitation and 630 nm emission. Signal for each well at any given time point was normalized to that for the same well at the start of the experiment. Oxygen concentrations were calculated from fluorescence values using the following formula: $[O_2] = (DR/NRF - 1)/K_{SV}$, where DR is the dynamic range, NRF is the normalized relative fluorescence, and K_{SV} is the Stern-Volmer constant, as detailed in Technical Bulletin #443 from BD Biosciences. Values in Figure 1D were expressed as nmol O_2 consumed/100,000 cells. The FO/F1 ATPase inhibitor Oligomycin (Sigma, working concentration 0.2 μg/ml) was added to OC316 or IGROV-1 cells to test coupling of O_2 consumption to ATP synthesis.

Lentiviral Vector-Mediated Transduction of shRNA in Ovarian Cancer Cells

The lentiviral plasmids containing HIF-1α shRNA expression cassette or an un-relevant shRNA sequence targeted to the *luciferase* gene (referred to as LUC thereafter)[21] were a kind gift of Dr. O.V. Razorenova (Department of Molecular Cardiology, Lerner Research Institute, Cleveland, OH). The lentiviral vectors were produced as previously de-

scribed.[22] Cells expressing the shRNA were selected in puromycin-containing medium. OC316 and IGROV-1 cells bearing the shRNA targeted to HIF-1α were termed OC316 ΔHIF-1α and IGROV-1 ΔHIF-1α, respectively; the corresponding cell lines bearing the shRNA targeted to LUC were termed OC316 control and IGROV-1 control. The plasmid pHIF-1α, kindly provided by S. Pennacchietti (Istituto per la Ricerca e la Cura del Cancro, Candiolo, Torino, Italy) was used in a set of experiments to transfect OC316 ΔHIF-1α cells using Lipofectamine 2000 (Invitrogen, Carlsbad, CA).

Proliferation Assays

To measure proliferation, IGROV-1 and OC316 parental cells or their derivatives were seeded in triplicate in 96-well flat-bottom plates at different densities (range, 1250 to 10,000 cells/well) and exposed to normoxia or hypoxia for 48 hours. In all experiments, 0.5 μCi thymidine was added to each well before incubation. Subsequently, the cells were harvested and [^{3}H] thymidine incorporation was evaluated by using a Scintillation Counter (Beckman Coulter, Fullerton, CA).

Cell Cycle Analysis

To evaluate cell cycle distribution after incubation under normoxic or hypoxic conditions for 48 hours, 3 to 5 × 10^5 OC316 HIF-1α proficient and deficient cells were washed with ice-cold PBS, re-suspended in 1 ml of Glucose-Modified solution (1.1 mmol/L glucose, 0.14 M NaCl, 5 mmol/L KCl, 1.5 mmol/L Na_2HPO_4, 1.1 mmol/L KH_2PO_4, 0.5 mmol/L EDTA), and fixed by the drop-wise addition of 3 ml of 100% ethanol for 20 minutes at 4°C. Subsequently, cells were washed twice with ice-cold PBS and re-suspended in 500 μl of a PI solution (100 μg/ml) containing DNase-free RNase (12 μg/ml) (Sigma). After 1 hour incubation at room temperature, cells were analyzed by flow cytometry (FACSCalibur, Beckton Dickinson) using a 488-nm Argon laser and FL2-A detection line. The DNA content frequency histograms were de-convoluted by using ModFit LT3.0 software (Verity Software House).

Immunoblotting

The cells exposed to the various treatments were harvested, lysed and subjected to SDS-polyacrylamide gel electrophoresis and blotting. Immunoreactivity levels were evaluated by hybridization using the following antibodies: mouse monoclonal antibody (mAb) anti-HIF-1α (1:250; Transduction Laboratories, Lexington, KY), anti-α-tubulin (1:3000; Sigma); rabbit anti-poly(ADP-ribose) polymerase (PARP) polyclonal antibody (1:1000; Cell Signaling Technology, Beverly, MA); and, anti-Rb or anti-phospho-Rb antibodies (1:1000; both from Cell Signaling Technology). The signal was then detected by chemiluminescence with SuperSignal kit (Pierce, Rockford, IL).

Reporter Gene Assays

Wild-type or mutant HRE luciferase-encoding plasmids were kindly provided by Dr. Celeste M. Simon (Department of Cell and Developmental Biology, Abramson Cancer Research Institute, Philadelphia, PA). OC316 cells were plated at 3.0 × 10^5 in six-well plates, and transiently transfected with 2 μg of wild-type HRE or mutant HRE constructs, and 0.5 μg of a β-gal control plasmid. Cells were allowed to recover for 24 hours, trypsinized, and seeded in triplicate in 96-well flat-bottom plates at different densities (range: 10,000 to 25,000 cells/well) and exposed to normoxia for 36 hours. Cells were then lysed and luciferase activity was analyzed with a luciferase assay kit (Promega, Madison, WI) according to the manufacturer's instructions. Luciferase values were normalized to β-gal activity, measured by the Galacto Light kit (Tropix, Bedford, MA).

Reverse Transcription PCR and Real-Time PCR Assay

Total RNA was extracted using the RNeasy Mini Kit (Qiagen, Hilden, Germany). cDNA was synthesized from 0.5 to 1 μg of total RNA using the Superscript II reverse transcriptase (Invitrogen). Real-time PCR was performed with SYBR Green dye and Gene AMP 5700 Sequence Detection System (PE Biosystems, Foster City, CA). Two μl of cDNA were used as template; 10 μl of 2× Platinum SYBR Green qPCR SuperMix-UDG (Invitrogen) were mixed with template and primers. The total reaction volume was 20 μl. Cycling conditions were 10 minutes at 95°C, 40 cycles of 15 seconds at 95°C, and 1 minute at 60°C. Each sample was run in duplicate. For all genes evaluated, mRNA was normalized to β_2-microglobulin (β_2-m) mRNA by subtracting the cycle threshold (Ct) value of β_2-m mRNA from the Ct value of the gene of interest (ΔCt). Fold difference ($2^{-}\Delta\Delta$Ct) was calculated by subtracting the ΔCt (treated sample) − ΔCt (reference sample), to generate a ΔΔCt. PCR efficiency was in the range 95% to 105%. The following primers were used for real-time PCR: human Hexokinase II (sense, 5′-GAAGATGCTGCCCACCTTTG-3′; antisense, 5′-CACCCAAAGCACACGGAAGT-3′), human glyceraldehyde-3-phosphate dehydrogenase (GAPDH) (sense, 5′-GAAGGTGAAGGTCGGAGT-3′; antisense, 5′-CATGGGTGGAATCATATTGGAA-3′), human lactate dehydrogenase (LDH)-A (sense, 5′-GATTCAGCCCGATTCCGTTAC-3′; antisense, 5′-ACTCCATACAGGCACACTGG-3′), human HIF-1α (sense, 5′-TCGGCGAAGTAAAGAATCTGA-3′; antisense, 5′-CAAATCACCAGCATCCAGAA-3′), human vascular endothelial growth factor (VEGF) (sense, 5′-AACCATGAACTTTCTGCTGTCT-3′; antisense, 5′-TTCACCACTTCGTGATGATTCT-3′), human cyclin D2 (sense, 5′-AACCTGCTCACCATCGAGGA-3′; antisense, 5′-TGGATGCTGGAGGTCTGTGA-3′), human p27 (sense, 5′-GCTCCGGCTAACTCTGAGGA-3′; antisense, 5′-AGAATCGTCGGTTGCAGGTC-3′), human β_2-m (sense, 5′-TGCTGTCTCCATGTTTGATGTATCT-3′; antisense 5′-TCTCTGCTCCCCACCTCTAAGT-3′).

Tumorigenicity Assays

SCID mice were purchased from Charles River (Wilmington, MA), and maintained in our animal facilities under pathogen-free conditions. Procedures involving animals and their care conformed to institutional guidelines that comply with national and international laws and policies (EEC Council Directive 86/609, OJ L 358, December 12, 1987).

To evaluate the effects of attenuation of HIF-1α expression on tumorigenesis, groups of 6 to 8-week-old SCID mice (n = 10/group) were injected subcutaneously (s.c.) in both flanks with OC316 ΔHIF-1α or control cells (5×10^4 cells/injection) mixed at 4°C with liquid Matrigel (Becton-Dickinson; final volume 300 μl/injection). Starting from the day of inoculation, the animals were inspected twice weekly and tumors measured by caliper; tumor volume was calculated as (length $\times$ width^2) $\times$ 0.5. In a set of experiments, OC316 ΔHIF-1α or control cells (1×10^6 cells/injection) were injected i.p. in SCID mice (n = seven mice/group).

At the end of the experiment, the mice were euthanized by cervical dislocation. The tumors were harvested by dissection, weighed and either snap-frozen or fixed in formalin and embedded in paraffin for immunohistochemistry or other analyses.

Optical Imaging of Tumors

To perform *in vivo* imaging, OC316 control and ΔHIF-1α were transduced with a lentiviral vector encoding the *EGFP* reporter gene[23] to obtain an EGFP$^+$ cell population. EGFP$^+$ cells were then injected s.c. in anesthetized SCID mice (600,000 cells in 100 μl PBS/flank). Immediately after injection, and at several time points thereafter, images were acquired using the eXplore Optix System (GE Health care, London, Canada) at a fixed integration time (0.3 seconds) and scan step (1.5 mm); laser power value (μW) was adapted to reach the 70% (Ph/sec) of maximum laser power. Analysis of images was performed using eXplore Optix OptiView software (GE Health care); a region of interest was manually selected around the signal intensity. Fluorescence was calculated as total intensity (normalized counts)/area (mm^2).

Histology and Immunohistochemistry

Four μm-thick tumor sections were rehydrated, and either stained with H&E or processed for immunohistochemistry.

Tumor vessels were labeled with a rat anti-CD31 mAb (1:50 dilution; Becton-Dickinson); immunostaining was performed using the avidin-biotin-peroxidase complex technique and 3–3′ diaminobenzidine as chromogen (Vector Laboratories, Burlingame, CA), and the sections were then lightly counterstained with Mayer's hematoxylin. Parallel negative controls obtained replacing primary antibodies with PBS were run in all cases. Microvessel density was quantified by screening the CD31-stained sections for the areas of highest vascularity. Cell proliferation was evaluated in formalin-fixed paraffin-embedded tumor sections by staining with the anti-Ki-67 antibody (Novocastra Laboratories, Newcastle, UK) according to the manufacturer's instructions. To determine microvessel density and cell proliferation ten representative fields at $\times$400 magnification for each tumor were counted. Magnification of $\times$100 was used for the analysis of necrosis.

Quantification of necrosis was performed by using the Laser Microdissection Software version 4.3 of a laser-assisted microdissector (AS-LMD Leica Microsystems, Wetzlar, Germany). Briefly, the sample was first completely scanned and divided in a variable number of identical fields, depending on its total surface. In every field, the total tumor area and the area of necrosis were measured by the software and expressed as μm^2. Finally, to calculate the percentage of necrotic areas, the sum of the necrotic areas in all fields was divided for the total area of the sample.

Evaluation of Hypoxia and Perfusion Markers

To identify hypoxic cells in tumors generated in SCID mice, we used pimonidazole hydrochloride (Hypoxyprobe-1; Chemicon International, Temecula, CA), which was administered to mice i.p. 1.5 hours before sacrifice at 100 mg/kg of body weight in saline. Tumor sections were immunostained to detect pimonidazole adducts following the manufacturer's instructions. To measure perfusion, mice were injected with dextran 70-fluorescein isothiocyanate (Invitrogen; 360 μM, 50 μl per mouse) 5 minutes before sacrifice.

For immunofluorescence analysis, 5 μm-thick paraffin-embedded or frozen tumor sections were washed three times with PBS and then incubated for 1 hour at room temperature with a saturating solution consisting of 5% goat serum, 1% bovine serum albumin, and 0.1% Triton-X in PBS. After saturation, slides were incubated with either Hypoxyprobe-1 mouse mAb (Chemicon International) or rat anti-CD31 (Becton-Dickinson), washed and incubated with the goat anti-mouse Alexa Fluor 488 or goat anti-rat 546 secondary antibody (both from Invitrogen), respectively.

Nuclei were stained with TO-PRO-3 iodide (Invitrogen; blue signal) for 15 minutes, before washing and mounting of coverslips on glass slides for microscopy. Confocal laser scanning microscopy was performed with a Zeiss LSM 510 microscope (Zeiss, Jena, Germany) using Argon (488 nm) and Helium-Neon (543 to 633 nm) laser sources. Analysis of tumor hypoxia was done by calculating the fraction of tumor area stained for the hypoxic marker pimonidazole; the number of fields analyzed varied between 5 and 10 per section, depending on the tumor size. Images were collected at a total magnification of $\times$100.

End-Point RT-PCR Analysis

Expression of angiogenic factors including VEGF, interleukin-8, GRO-α, and COX-2 was investigated in OC316 ΔHIF-1α or control OC316 tumors. Equivalent amounts of RNA obtained from two pools of three tumors of each type were used for cDNA synthesis.

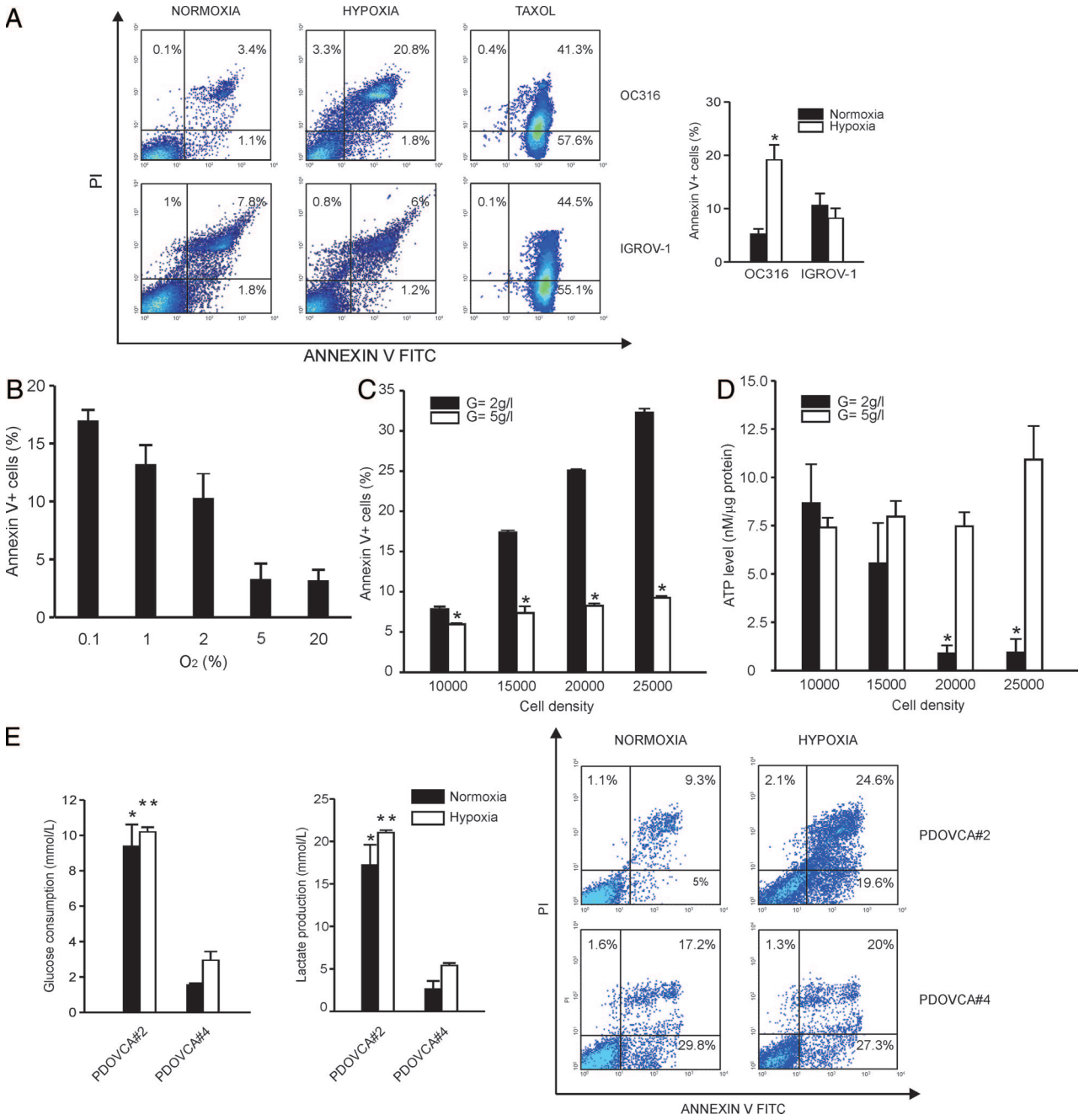

Figure 2. Correlation between hypoxia-induced cell death and the glycolytic phenotype in ovarian cancer cells. **A:** Hypoxia-induced cell death in ovarian cancer cells. Cells were plated in P6 wells at 1.5×10^5 cells/well. Following 72 hours incubation under normoxic or hypoxic conditions, the cells were labeled with Annexin V/PI and the level of cell death was measured by flow cytometry. The left panels show representative diagrams of hypoxia-sensitive (OC316) and hypoxia-resistant (IGROV-1) cells. To illustrate the differences in cell death features, a diagram showing apoptosis in ovarian cancer cells treated with taxol is also shown. In the right panels, mean ± SD values of $n = 6$ (OC316) or $n = 7$ (IGROV-1) different experiments is reported. *Statistically significant differences in the percentage of Annexin V+ OC316 cells under hypoxic versus normoxic conditions ($P < 0.05$). **B:** Levels of hypoxia-induced cell death in OC316 cells under various oxygen concentrations. OC316 cells were plated and incubated as detailed above by varying the levels of O_2 in the hypoxic chamber. Annexin V binding was measured by flow cytometric analysis. Mean ± SD values of two experiments are shown. **C:** Glucose supplementation protects cancer cells from death under hypoxic conditions. OC316 cells were grown for 48 hours under hypoxic conditions with standard (2 g/L, low) or increased (5 g/L, high) glucose concentrations in the medium. Cell death was measured by measuring Annexin V/PI staining. Mean ± SD of five different experiments is shown. *Statistically significant differences in the percentage of Annexin V+ OC316 cells cultured in low- versus high-glucose medium ($P < 0.05$). **D:** Hypoxia-induced cell death depends on exhaustion of ATP levels and it is cell density–dependent. Cells were grown for 48 hours followed by measurement of intracellular ATP levels. The number of cells seeded in individual wells is reported on the *x* axis. ATP measurements were done in triplicate. Mean ± SD of five experiments is shown. *Statistically significant differences in the ATP levels in OC316 cells cultured in low- versus high-glucose medium ($P < 0.05$). **E:** Cellular responses of primary ovarian cancer cell cultures to hypoxia. Left panel, measurement of glucose consumption and lactic acid production by two primary epithelial ovarian cancer cultures from xenografts. Supernatants were collected after 24 hours *in vitro* culture under either normoxic or hypoxic conditions and metabolic parameters quantified by an automatic analyzer. Values were normalized to cell counts at time of collection of the supernatants. Mean ± SD of three experiments is shown. Statistically significant differences between PDOVCA#2 and PDOVCA#4 cells under normoxic (*) or hypoxic (**) conditions ($P < 0.05$). Right panel, detection of hypoxia-induced cell death in primary epithelial ovarian cancer cells. Following 72 hours incubation in the presence of 0.3% O_2, the cells were labeled with Annexin V/PI and the level of cell death was measured by flow cytometry. The panels show representative diagrams of both hypoxia-sensitive (PDOVCA#2) and hypoxia-resistant (PDOVCA#4) cells.

Primer sequences and RT-PCR conditions have been reported elsewhere.[24]

Imaging Bioluminescence

For quantitative measurement of lactate and ATP, the technique of bioluminescence imaging was applied, as described before.[25,26] Briefly, reaction solutions containing specific enzymes that link lactate and ATP to the luciferase of *Photobacterium fischeri* and *Photinus pyralis*, respectively, were applied to tumor cryosections. Light emission was induced at 20°C in a temperature-stabilized reaction chamber, which was placed under an appropriate microscope (Axiophot, Zeiss, Oberkochen, Germany) connected to a 16-bit CCD camera with an imaging photon counting system (C2400, Hamamatsu, Herrsching, Germany). The resulting images of the spatial distribution of light intensities were calibrated using appropriate standards. Images were displayed in colors coding for tissue concentration of metabolites in units of μmol/g. Computerized image analysis allowed for separate data assessment in selected histological areas of xenotransplanted tumors. ATP and lactate concentrations were ascertained exclusively from vital tumor regions.

Statistical Analysis

Results were expressed as mean value $\pm$ SD. Statistical analysis was performed using Student's *t*-test and the non-parametric test Mann-Whitney Wilcoxon test. Differences were considered statistically significant at $P < 0.05$.

Results

Assessment of the Metabolic Properties of Different Ovarian Cancer Cell Lines

In preliminary experiments, we identified two ovarian cancer cell lines, OC316 and IGROV-1, which had different metabolic profiles, based on the expression of genes involved in glycolysis, including HKII, GAPDH, and LDH-A, which was 7- to 16-fold higher in OC316 cells compared to IGROV-1 cells (Figure 1A). Furthermore, the rates of glucose consumption and lactate production *in vitro* were significantly higher in OC316 than in IGROV-1 cells (Figure 1B). Consistent with these findings, an analysis of the kinetics of lactate production showed an increased rate of lactate production by OC316 compared to IGROV-1 cells (Figure 1C). Proliferation of OC316 and IGROV-1 cells *in vitro* was similar (not shown).

To further investigate the metabolic profiles of these cells, we next tested their O_2 consumption rates using a fluorimetric assay. Results showed similar levels of O_2 consumption in OC316 and IGROV-1 cells during the time course of the experiment (Figure 1D). Interestingly, for both cell lines oxygen consumption was completely inhibited by oligomycin, a drug that blocks the F0/F1 ATPase, indicating that O_2 consumption was tightly coupled to ATP production in both cell lines (Figure 1D).

To investigate whether the results described so far could be due to differences in the metabolic rate/ATP demand of OC316 and IGROV-1 cells, we measured the rate of ATP depletion following acute deprivation of substrates, ie, glucose, pyruvate and glutamine. To minimize the impact on these measurements of ATP synthesis from endogenous carbohydrate, lipid, and amino acid catabolism, we focused on the very early phases of this process. Results, shown in Figure 1E, indicate that the rate of ATP decay in the first 2 minutes were similar in both cell types (1.41 $\pm$ 0.11 and 1.20 $\pm$ 0.41 nmol/L ATP/min/μg protein in OC316 and IGROV-1 cells, respectively). This result suggests that the two cell lines did not differ significantly in their ATP utilization rate (Figure 1E). In addition, measurements of steady-state ATP levels in standard culture conditions revealed no significant difference between IGROV-1 and OC316 cells (Figure 1E). The fact that both the steady state concentration and consumption rate of ATP was similar in IGROV-1 and OC316 cells suggests that the rate of ATP production is also likely to be similar in these cell lines.

Hypoxia-Induced Cell Death Correlates with the Metabolic Properties of Ovarian Cancer Cells

We then evaluated the responses to hypoxia of OC316 and IGROV-1 cells. Following 72 hours incubation in the presence of 0.3% O_2, cells were labeled with Annexin V/PI and the level of cell death was measured by flow cytometry. In 6 independent experiments, hypoxia increased levels of Annexin V-positive OC316 cells from 5.3 $\pm$ 1.0% to 19.2 $\pm$ 2.8%; interestingly, we detected mainly Annexin V+/PI+ OC316 cells (Figure 2A), indicating that cell death under these conditions had predominant features of late apoptosis. To determine the response of OC316 cells to less extreme conditions of hypoxia we performed an oxygen dose-response experiment. Results, shown in Figure 2B, indicate that OC316 cells maintain their sensitivity to hypoxia-induced cell death also under 1% or 2% O_2. Interestingly, IGROV-1 cells, which exhibit lower rates of glucose consumption/lactate production than OC316 cells (Figure 1, B and C) were also resistant to hypoxia-induced cell death: Annexin V-positive IGROV-1 cells were 10.7 $\pm$ 2.2% and 8.3 $\pm$ 1.8% under normoxic and hypoxic conditions, respectively (Figure 2A). In contrast, the cytotoxic drug taxol caused similar levels of cell death in IGROV-1 and OC316 cells (Figure 2A).

Because the hypoxia-sensitive OC316 cells depleted glucose more rapidly from the medium than IGROV-1 cells, we hypothesized that reaching a critical glucose concentration may be key in determining the onset of cell death. In support of this hypothesis, we found that cell death correlated with the number of cells plated and glucose supplementation rescued OC316 cells from death under hypoxic conditions (Figure 2C). Moreover, intracellular ATP levels inversely correlated with cell den-

sity under hypoxic conditions and their reduction was prevented by glucose supplementation (Figure 2D). In conclusion, under these experimental conditions tumor cell death was clearly associated with substrate depletion and ATP deprivation.

Finally, we extended these studies to two primary cultures established from ovarian cancer xenografts. In this case as well, PDOVCA#2 cultures, which exhibit higher glucose consumption/lactate production rates, were more sensitive to hypoxia-induced cell death than PDOVCA#4 cells that are characterized by lower glucose consumption/lactate production rates (Figure 2E). These data indicate that also in the context of primary cultures established from tumors the metabolic profile is a key factor determining sensitivity to hypoxia-induced cell death.

Modulation of Hypoxia-Induced Cell Death by HIF-1α Is Dependent on Cell Metabolism

The hypoxia-regulated transcriptional factor HIF-1α has been reported to contribute to either pro-apoptotic or anti-apoptotic effects in different experimental systems and to shift cell metabolism toward glycolysis (reviewed in:[7]). To address the role of HIF-1α in determining survival versus death under hypoxic conditions in our model, we generated HIF-1α knock-down IGROV-1 and OC316 cell lines (IGROV-1 ΔHIF-1α and OC316 ΔHIF-1α). These cell lines were obtained by transduction of shRNAs targeted to HIF-1α by lentiviral vectors previously described.[21] The levels of HIF-1α mRNA in IGROV-1 ΔHIF-1α and OC316 ΔHIF-1α cells were reduced by 80 to 90% compared to controls, as measured by quantitative PCR analysis (Figure 3A); moreover, HIF-1α protein was virtually undetectable by Western blot analysis in IGROV-1 ΔHIF-1α, and OC316 ΔHIF-1α even following treatment with the hypoxia-mimetic drug $CoCl_2$ (Figure 3B). Expression of the VEGF transcript, which is regulated by HIF-1α, was increased by 2- to 4-fold under hypoxia in controls and much less in IGROV-1 ΔHIF-1α, and OC316 ΔHIF-1α cells (Figure 3C), thus confirming the reduction of functional HIF-1α in these cells. Transfection of OC316 and IGROV-1 cells with a HRE-luciferase expression plasmid confirmed the presence of functional HIF-1 in both cell lines, and its marked reduction following silencing with the HIF-1α-targeting vector (data not shown).

Ovarian cancer cells bearing different levels of HIF-1α expression disclosed heterogeneous responses to acute hypoxia: in fact, HIF-1α silencing increased apoptosis of OC316 cells under hypoxic conditions, whereas IGROV-1 cells remained substantially resistant to hypoxia-induced cell death regardless of their HIF-1α status (Figure 4A). Culture of OC316 ΔHIF-1α cells in medium with high glucose concentrations reverted the effects of hypoxia on cell viability (Figure 4A). To determine whether the effect on cell death observed was a consequence of the inactivation of HIF-1α, a plasmid encoding HIF-1α was introduced into OC316 ΔHIF-1α cells by transient transfection: forced expression of HIF-1α restored the levels of

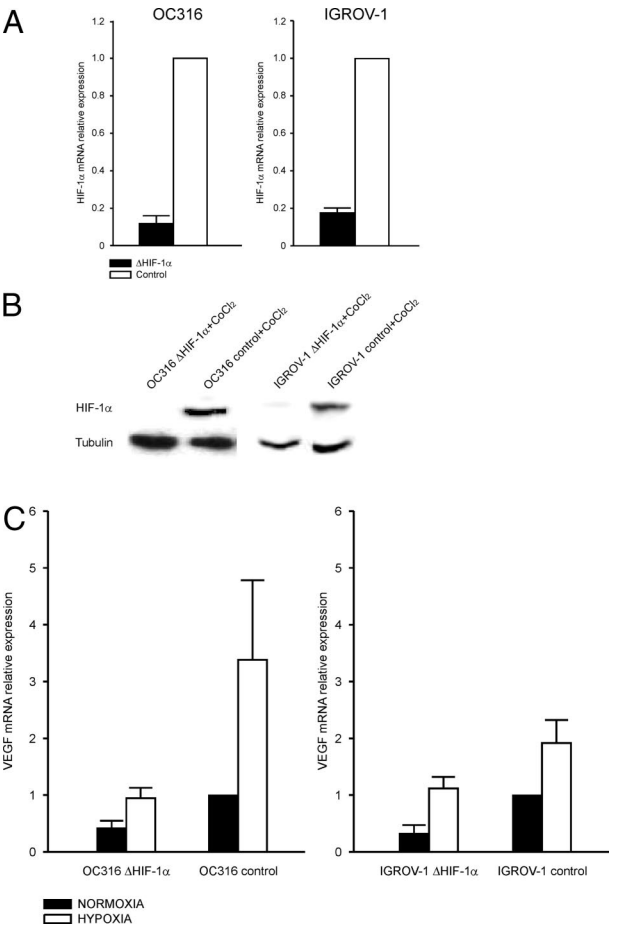

Figure 3. Stable silencing of HIF-1α by lentiviral vector-mediated transfer of shRNA in ovarian cancer cells. **A:** Reduction of HIF-1α transcripts levels in IGROV-1 ΔHIF-1α and OC316 ΔHIF-1α cells by quantitative RT-PCR analysis. Mean ± SD of three different transduction experiments is shown. **B:** Detection of HIF-1α protein by Western blot analysis in lysates of OC316 and IGROV-1 transduced cells incubated in the presence of the hypoxia-mimetic drug $CoCl_2$. Tubulin was used as a loading control. **C:** Measurement of expression of HIF-1-controlled gene VEGF in OC316 and IGROV-1 cell derivatives by quantitative PCR analysis. Mean ± SD of three different experiments performed is shown.

hypoxia sensitivity measured in control OC316 cells (Figure 4A). These results confirmed the specificity of HIF-1α knockdown approach and ruled out off-target effects as responsible for the survival effect. Analysis of the amounts of cleaved PARP in cell lysates by immunoblotting (Figure 4B) reinforced the evidence that HIF-1α attenuation promoted OC316 cell death under low oxygen concentration.

Based on our findings with parental OC316 cells, showing a correlation between the onset of hypoxia-induced cell death and a sharp reduction of intracellular ATP levels (see Figures 1 and 2), we sought to investigate the influence of HIF-1α silencing on this effect. As expected, OC316 control cells underwent a marked reduction of intracellular ATP in a density-dependent fashion under hypoxic conditions (Figure 4C, left top panel); intriguingly, OC316 ΔHIF-1α cells disclosed a similar behavior but this occurred at a lower cell density compared to HIF-1α proficient cells. In any case, these variations in ATP levels in both OC316 ΔHIF-1α and control cells were prevented by increasing the glucose concentration of the

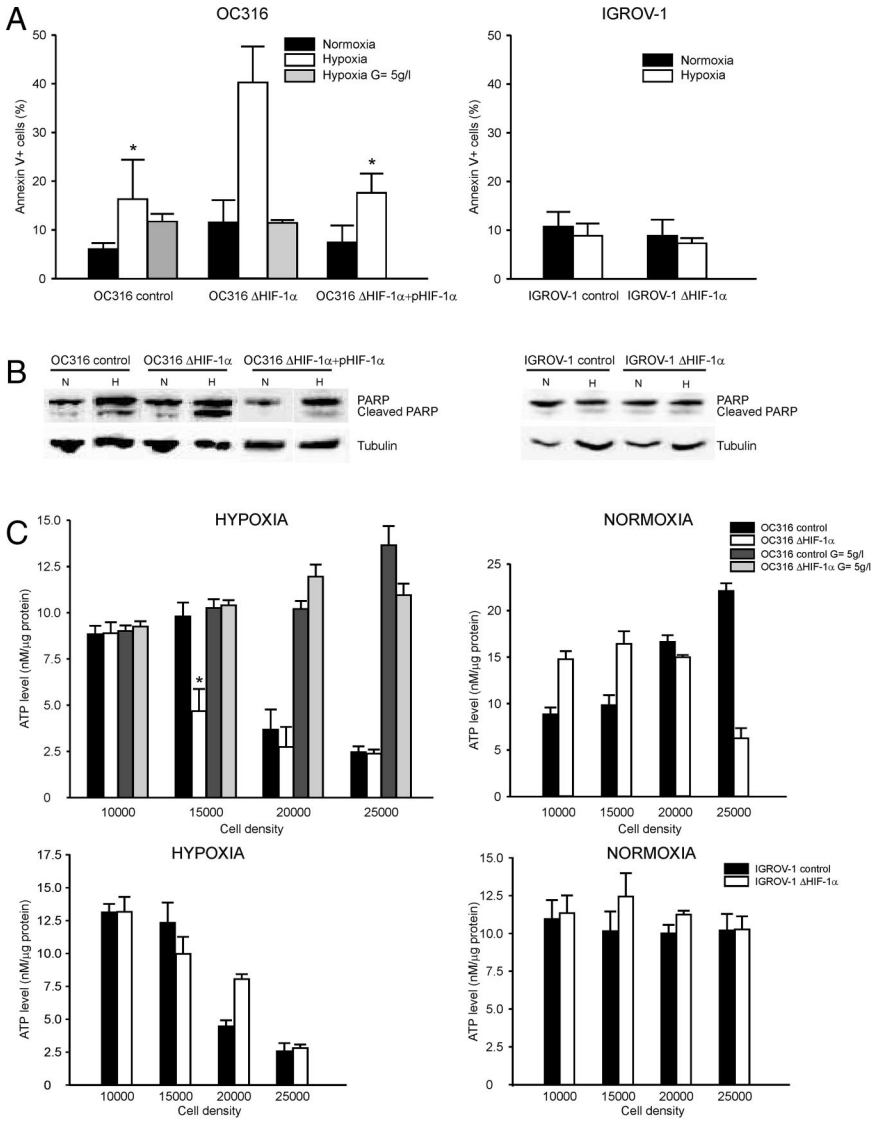

Figure 4. Hypoxia-induced cell death in cancer cells bearing attenuated HIF-1α expression is associated with anticipated depletion of intracellular ATP levels. **A:** Flow cytometric analysis of annexin V+ cells following 72 hours incubation in normoxic or hypoxic conditions. The plasmid pHIF-1α was used to transfect OC316 ΔHIF-1α cells and obtain HIF-1α-complemented cells as described in the Materials and Methods. Mean ± SD of three different experiments is shown. *Statistically significant differences in the percentage of Annexin V+ OC316 control or HIF-1α-complemented cells versus OC316 ΔHIF-1α cells under hypoxic conditions ($P < 0.05$). **B:** Western blot analysis of the amounts of cleaved PARP forms in cell lysates of samples treated as described in (**A**). Equivalent amounts of proteins were immunoblotted with anti-PARP and anti-tubulin as loading control. **C:** Effects of HIF-1α silencing on the energy status of epithelial ovarian cancer cells: measurement of intracellular ATP levels following 48 hours incubation under either normoxic or hypoxic conditions. OC316 (top panels) and IGROV-1 cells (botton panels) were plated at various densities in 96-well plates, with normal (2 g/L) or high (5 g/L) glucose concentrations. ATP measurements were done in triplicate. Mean ± SD of 1 representative experiment out of five performed is shown. *Statistically significant differences in ATP levels between OC316 ΔHIF-1α and control cells ($P < 0.05$). **D:** ATP consumption rates in OC316 ΔHIF-1α and control cells. Cells were incubated under normoxic or hypoxic conditions as reported in the Materials and Methods. The columns report the results of three independent experiments, as variation in the ATP levels (%) after 30 minutes incubation in D5030 medium. Mean ± SD of three experiments is shown. *Statistically significant differences in ATP consumption rates between OC316 ΔHIF-1α and control cells in hypoxic conditions ($P < 0.05$).

medium (Figure 4C, left top panel). A similar difference in ATP levels was measured also under normoxic conditions at high cell densities (Figure 4C, right top panel), which suggested that HIF-1α could be expressed even under normoxic conditions. HIF-1α, however, was undetectable by Western blot analysis in OC316 cells cultivated at various densities under normoxic conditions (Supplementary Figure S1 at *http://ajp.amjpathol.org*). Moreover, transfection of OC316 cells with HRE-luciferase constructs did not show a substantial increase in luciferase activity by increasing cell density, thus implying that only low levels of functional HIF-1α protein were conceivably present in normoxic OC316 cells (Supplementary Figure S1 at *http://ajp.amjpathol.org*).

In contrast, no substantial changes in ATP levels were measured in IGROV-1 cell derivatives under normoxic conditions at any of the cell densities considered (Figure 4C, right bottom panel), while under hypoxic conditions a reduction of ATP levels at high cell densities was measured, but with a similar trend in HIF-1α deficient and proficient cells (Figure 4C, left bottom panel).

Importantly, ATP consumption rates were similar in OC316 ΔHIF-1α and control cells under normoxic conditions: in contrast, ATP levels decreased more rapidly in OC316 ΔHIF-1α cells compared to control cells under hypoxic conditions, thus suggesting that HIF-1α inactivation could modulate the ATP demand of these cells (Figure 4D).

We finally measured the expression of glycolytic genes HKII, GAPDH, and LDH-A in control or HIF-1α knock-down OC316 cells. Results showed that HIF-1α silencing prevented the increase in the HKII, GAPDH, and LDH-A expression under hypoxic conditions, while it had less marked effects on the expression levels of these genes in normoxic conditions (Supplementary Figure S2A at *http://ajp.amjpathol.org*). Accordingly, lactate levels were lower in OC316 ΔHIF-1α cell cultures than in control cells under hypoxic conditions and glucose levels had opposite variations (Supplementary Figure S2B at *http://ajp.amjpathol.org*), but differences were not significant. Thus, HIF-1α silencing did not impair markedly the glycolytic capacity of OC316 cells, implying that other genes are likely involved.

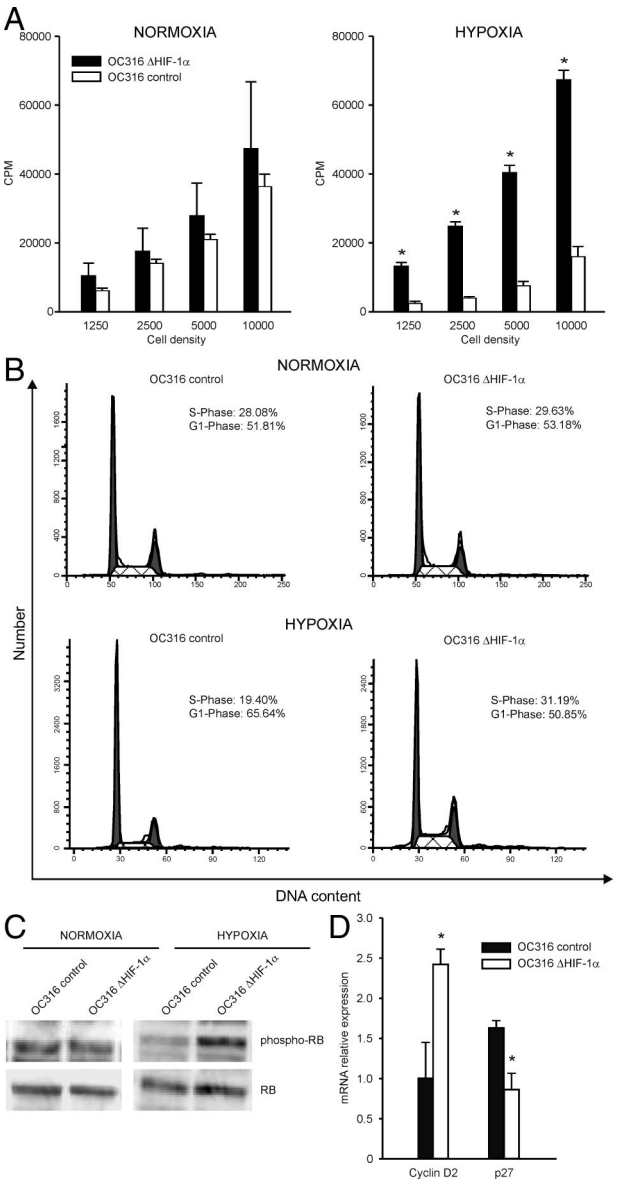

Figure 5. HIF-1α inactivation removes a brake to cell proliferation under hypoxic conditions in ovarian cancer cells. **A:** Proliferation of OC316 cells with different HIF-1α status by the [^{3}H] thymidine assay after 48 hours incubation under normoxic or hypoxic conditions. Mean ± SD of three experiments is shown. *Statistically significant differences in the cpm values in OC316 control versus OC316 ΔHIF-1α cells under hypoxic conditions ($P < 0.05$). **B:** Cell cycle analysis of OC316 ΔHIF-1α or control cells following 48 hours incubation under normoxic or hypoxic conditions. One representative experiment is illustrated. **C:** Western blot analysis of the phosphorylated and non-phosphorylated Rb protein in lysates from OC316 cell derivatives under different experimental conditions. One representative experiment of two is shown. **D:** Expression of c-Myc target genes (Cyclin D2 and p27) under hypoxic conditions by quantitative PCR analysis. Expression of each gene was normalized to the β2-microglobulin transcript, used as house-keeping gene. The expression levels in OC316 control cells under normoxic conditions were then set at 1 and relative expression levels were calculated. Mean ± SD of three experiments is shown. *Statistically significant differences in OC316 control versus OC316 ΔHIF-1α cells under hypoxic conditions ($P < 0.05$).

HIF-1α Silencing Removes a Brake to Cell Proliferation under Hypoxic Conditions

The increased ATP consumption by HIF-1α deficient cells in hypoxia prompted us to measure proliferation of OC316 variants. Proliferation of OC316 cells bearing normal levels of HIF-1α was comparable to that of OC316 cells lacking HIF-1α under normoxic conditions at various cell densities (Figure 5A), as evaluated by the [^{3}H] thymidine proliferation assay. Under hypoxic conditions, proliferation of control OC316 cells was significantly reduced compared to normoxic conditions (Figure 5A). In contrast, OC316 cells devoid of HIF-1α maintained values similar or even higher than those measured under normoxic conditions (Figure 5A). As HIF-1α has been reported to be involved in hypoxia-induced arrest of cell proliferation,[27–29] we investigated the cell cycle profile of OC316 cells bearing different levels of HIF-1α expression. As expected, under hypoxic conditions control OC316 cells underwent a reduction in the S-phase, and a corresponding increase in the G1-phase (Figure 5B, and Supplementary Table S1 at *http://ajp.amjpathol.org*); on the other hand, OC316 cells lacking HIF-1α had similar profiles under normoxic and hypoxic conditions (Figure 5B, and Supplementary Table S1 at *http://ajp.amjpathol.org*). The failure of OC316 ΔHIF-1α to slow down proliferation under hypoxic conditions was further shown by quantification of the ratio of phospho-Rb to Rb by Western blot analysis that indicated higher levels of phospho-Rb in OC316 ΔHIF-1α compared to control cells under hypoxic conditions (Figure 5C). HIF-1α may antagonize c-Myc activity by altering its interaction with its cofactor Sp1.[30] To investigate the role of c-Myc in these cell cycle changes, we assessed expression of the c-Myc targets p27 and Cyclin D2 in hypoxia.[31] Under the conditions described above, we measured lower levels of the p27 transcript (repressed by c-Myc) in OC316 ΔHIF-1α compared to control cells under hypoxic conditions (Figure 5D). Moreover, we observed the opposite effect on cyclin D2 (activated by c-Myc) levels, which were higher in OC316 ΔHIF-1α cells compared to control cells under hypoxic conditions (Figure 5D). Although the variations measured are relatively small, in accordance with other studies,[31] these results suggest that a higher c-Myc activity may contribute to confer increased proliferative activity to OC316 ΔHIF-1α cells.

Effects of Tumor Cell Metabolism on the Pathological Features of Tumors Bearing Attenuated Levels of HIF-1α Expression

According to these findings, inactivation of the HIF-1α pathway seemed to favor cell proliferation and precipitate cell death due to depletion of ATP; this was particularly evident in the case of OC316 cells. To investigate whether the HIF-1α status could modulate tumorigenicity of these cells, SCID mice were injected s.c. with ΔHIF-1α or control OC316 cells and tumor growth curves were determined. OC316 ΔHIF-1α tumors grew with similar kinetics as control tumors; at sacrifice, tumors volume and weight were comparable (Figure 6A). To further explore possible differences in growth rates between HIF-1α proficient and deficient cells, we labeled them with EGFP and followed tumor growth by optical imaging. This allowed us to track tumor growth *in vivo* at very early

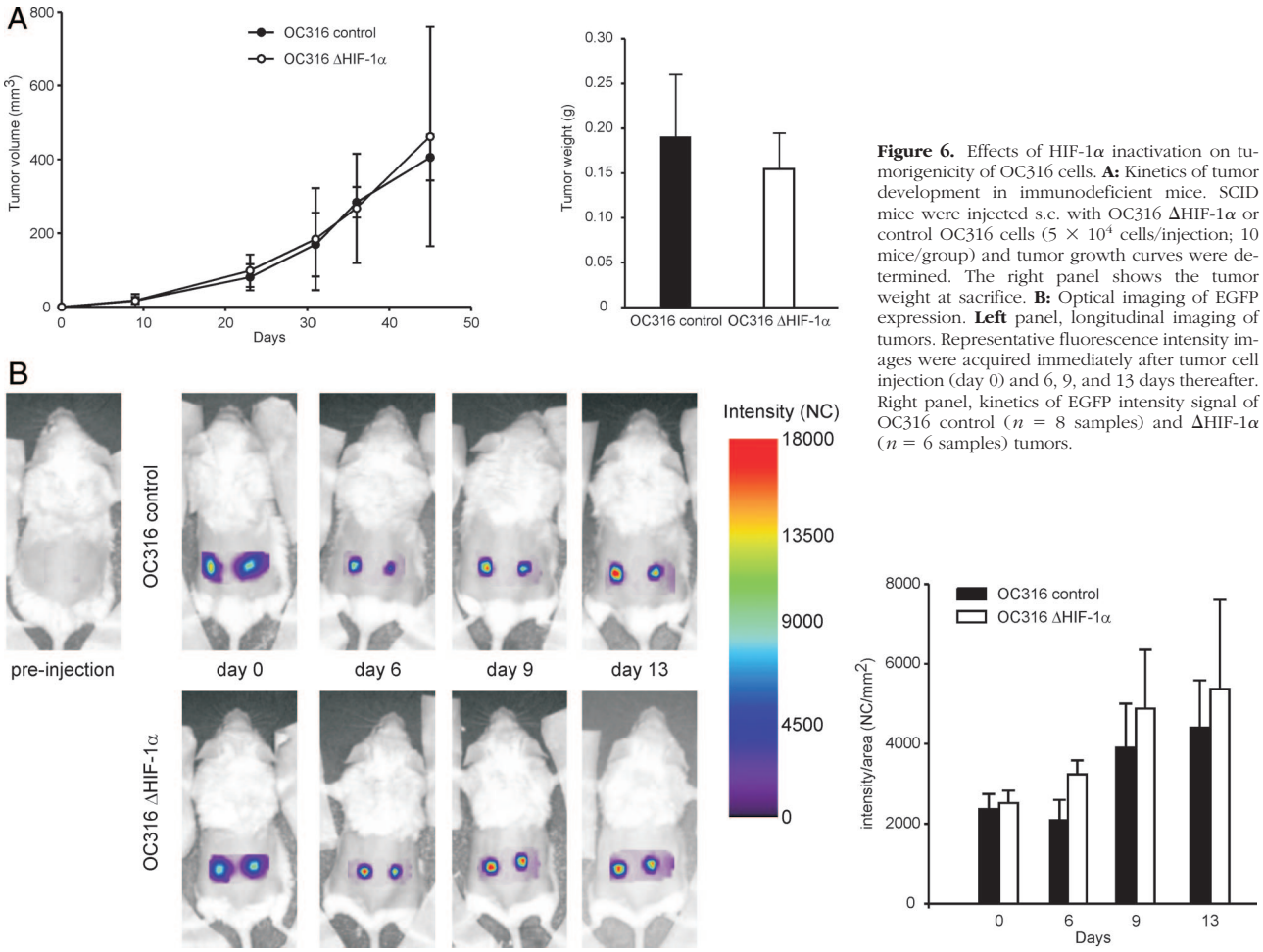

Figure 6. Effects of HIF-1α inactivation on tumorigenicity of OC316 cells. **A:** Kinetics of tumor development in immunodeficient mice. SCID mice were injected s.c. with OC316 ΔHIF-1α or control OC316 cells (5×10^4 cells/injection; 10 mice/group) and tumor growth curves were determined. The right panel shows the tumor weight at sacrifice. **B:** Optical imaging of EGFP expression. **Left** panel, longitudinal imaging of tumors. Representative fluorescence intensity images were acquired immediately after tumor cell injection (day 0) and 6, 9, and 13 days thereafter. Right panel, kinetics of EGFP intensity signal of OC316 control ($n = 8$ samples) and ΔHIF-1α ($n = 6$ samples) tumors.

time-points following injection. As shown in Figure 6B, we found that OC316 ΔHIF-1α tumors grew slightly faster than control tumors during the first 13 days after injection. Altogether, these findings indicated that HIF-1α silencing did not impair tumor growth and hinted at a gain of proliferative activity by OC316 ΔHIF-1α cells *in vivo*.

Expression of HIF-1α was checked in all tumors by quantitative PCR analysis, and a 75% reduction of HIF-1α expression in OC316 ΔHIF-1α compared to OC316 control tumors was found (data not shown). Histological analysis demonstrated a striking difference in the areas of necrosis, which were 22.5 ± 2.5% and 50.8 ± 9.5% in OC316 control and OC316 ΔHIF-1α tumors, respectively ($P < 0.05$, Figure 7A). Hypoxic areas were comparable in OC316 control and OC316 ΔHIF-1α tumors (38.24 ± 11.24% and 32.54 ± 12.23%, respectively), as measured by pimonidazole staining (Figure 7B). The proliferative activity in viable tumor regions was measured by Ki-67 staining and it was significantly increased in tumors lacking HIF-1α (Figure 7C), thus confirming the differences previously observed *in vitro*. Importantly, OC316 ΔHIF-1α tumors had similar microvessel density values as control tumors (Figure 7D), which, along with the similar percentage of hypoxic areas, suggested that the observed differences in necrosis between the two groups of tumors were not likely due to impaired angiogenic capacity of tumor cells lacking HIF-1α. This was also indicated by RT-PCR analysis, which demonstrated similar levels of transcripts of several angiogenic factors, including interleukin-8, GRO-α, and COX-2 in the two tumor groups (Figure 7E). The VEGF transcript was also detected, and it was only marginally decreased in OC316 ΔHIF-1α compared to control tumors (Figure 7E).

Finally, analysis of tumors formed by these cells in the peritoneal cavity, a location that could be clinically relevant, confirmed these findings by indicating similar kinetics of tumor development and increased areas of tumor necrosis in OC316 ΔHIF-1α compared to control tumors (Supplementary figure S3 at *http://ajp.amjpathol.org*). In conclusion, these findings highlight that HIF-1α inactivation is per se insufficient to delay ovarian cancer growth, although it can significantly increase tumor necrosis in the context of highly glycolytic cancer cells.

Metabolic Imaging of Tumors Bearing Attenuated Expression of HIF-1α

As inactivation of HIF-1α caused accelerated ATP consumption associated with increased proliferation under hypoxic conditions, we found it interesting to evaluate ATP and lactate levels in OC316 tumors. Figure 8A shows

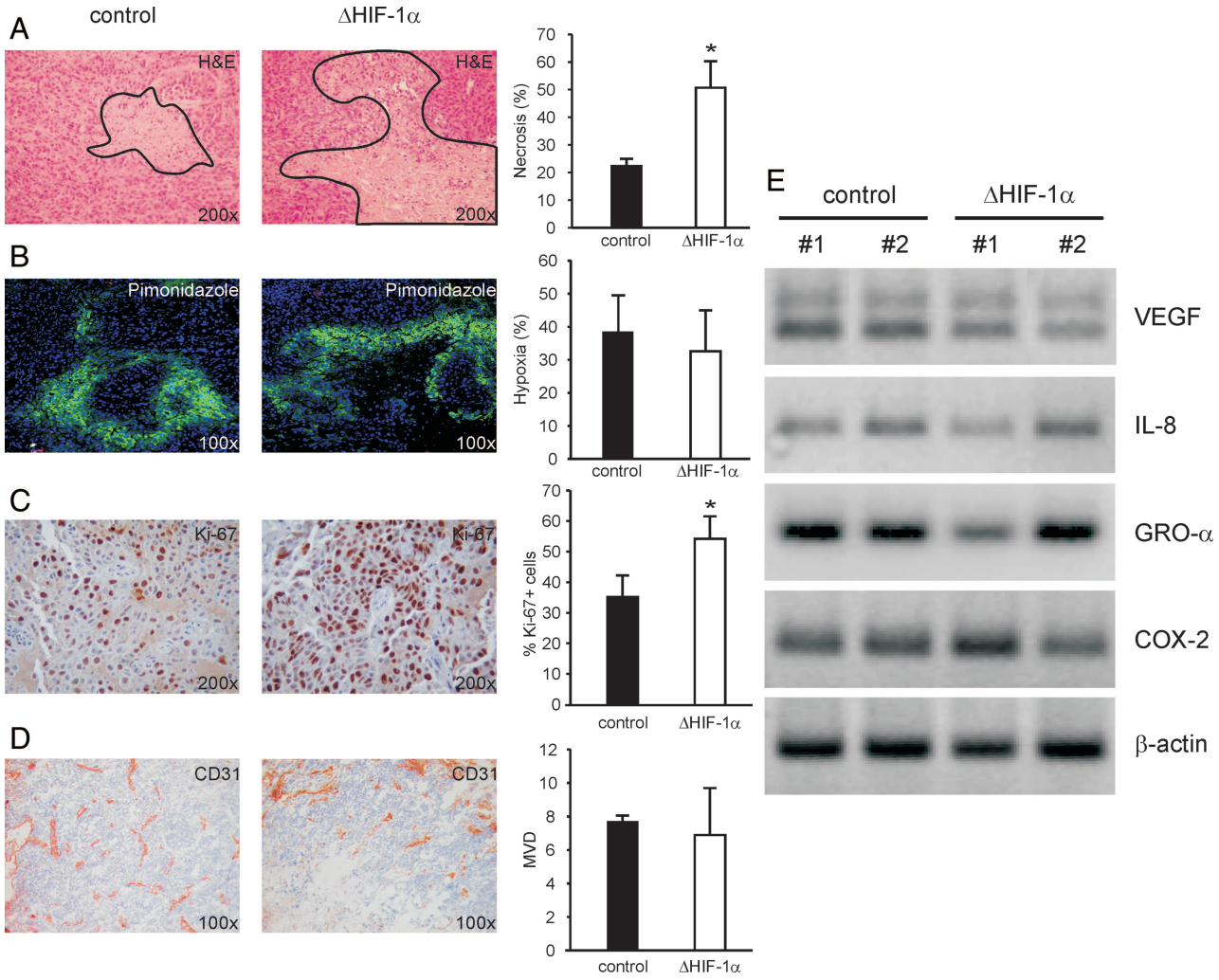

Figure 7. Effects of HIF-1α inactivation on morphological parameters of tumors. **A:** Histological analysis of OC316 control and OC316 ΔHIF-1α tumors shows larger necrotic areas in tumors bearing reduced levels of HIF-1α expression. Representative images (original magnification: ×200) are shown. The continuous line marks the boards of necrotic tissue. The columns on the right indicate quantitative analysis of necrotic areas in five samples of each experimental group. *Statistically significant differences in percentage of necrotic areas in OC316 control versus OC316 ΔHIF-1α tumors ($P < 0.05$). **B:** Evaluation of hypoxia by pimonidazole adducts staining. Representative images (original magnification: ×100) are shown. The columns on the right indicate quantitative analysis of hypoxic areas (defined as those stained positive for pimonidazole) in five samples of each experimental group. **C:** Evaluation of proliferation in tumors by Ki-67 staining. Representative images (original magnification: ×200) are shown. The columns on the right indicate quantitative analysis of proliferation in six samples of each experimental group. *Statistically significant differences between OC316 control and OC316 ΔHIF-1α tumors ($P < 0.05$). **D:** Vascularization of OC316 ΔHIF-1α or control OC316 tumors by staining with anti-CD31 mAb and calculation of the microvessel density as described in the Materials and Methods. **E:** Expression of angiogenic factors including VEGF, interleukin-8, GRO-α and COX-2 in OC316 ΔHIF-1α or control OC316 tumors. Equivalent amounts of RNA obtained from two pools of three tumors of each type were used for cDNA synthesis and analyzed by RT-PCR. Bands were visualized on agarose gels following ethidium bromide staining.

results of metabolic imaging of representative sequential cryosections of OC316 ΔHIF-1α and OC316 control tumors with color-coded distributions of ATP and lactate concentrations. In agreement with the metabolic properties of OC316 cells *in vitro*, ATP levels were rather low in both group of tumors compared to head and neck xenotransplanted tumors analyzed in previously reported experiments.[32] Notably, HIF-1α deficient tumors showed high average lactate concentrations in vital tumor regions, which were comparable to those of control tumors (Figure 8B). Conversely, ATP levels were low both in HIF-deficient and the control tumors (Figure 8B). The finding that tumors formed by OC316 ΔHIF-1α cells remain highly glycolytic could be related to the increased proliferative activity of these cells in the hypoxic microenvironment, which may increase the metabolic demand of the tumor mass.

Discussion

The HIF-1α pathway is invariably activated under hypoxic conditions and orchestrates a complex transcriptional program ultimately finalized to enhance cell survival in a transiently unfavorable microenvironment.

Although the consequences of HIF-1α inactivation in cancer cells have been investigated in depth (reviewed in:[1,33,34]), there was a lack of studies aimed at clarifying the role of HIF-1α in the survival of cancer cells with different metabolic properties.

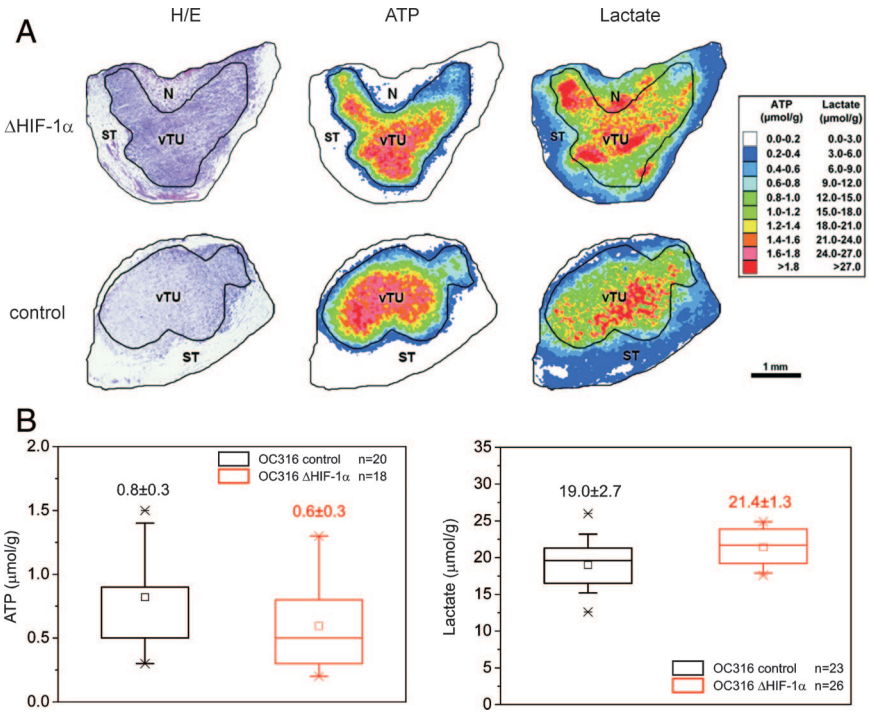

Figure 8. Metabolic imaging of tumors. **A:** H&E staining as well as color-coded distributions of ATP and lactate in sequential cryosections from a representative OC316 ΔHIF-1α and an OC316 control tumor. The concentration values were color-coded, with each color corresponding to a defined concentration range in μmol/g. For structure-associated evaluation different histological areas were delineated, such as vital tumor tissue (vTU), stromal elements (ST), and necrosis (N). **B:** Metabolite concentrations (mean ± SD) in OC316 ΔHIF-1α and OC316 control tumors derived from vital tumor regions exclusively. ATP: $n = 20$ for cryosections from seven different tumors of OC316 control and $n = 18$ for OC316 ΔHIF-1α. Lactate: $n = 23$ for cryosections from eight different tumors of OC316 control and $n = 26$ for OC316 ΔHIF-1α.

Expression of HIF-1α has previously been documented in ovarian cancer, both at the mRNA[35] and protein levels.[36,37] HIF-1α overexpression alone, however, has no impact on the prognosis of ovarian cancer unless accompanied by loss of functional p53, which identifies a subset of patients with dismal prognosis.

In our study, we observed heterogeneous metabolic phenotypes in the ovarian cancer cell lines analyzed. The mechanisms sustaining the marked metabolic differences observed remain currently unknown. Importantly, HIF-1α protein was not detected in IGROV-1 and OC316 cells under normoxic conditions by Western blot analysis, thus excluding that HIF-1α stabilization could account for the metabolic differences measured (Supplementary Figure S1 at *http://ajp.amjpathol.org*). One recent study showed that p53 may regulate the balance between the utilization of respiratory and glycolytic pathways through its downstream mediator SCO2.[38] We thus determined the p53 status of some of the cell lines used and found that OC316 and PDOVCA#2 cells, which are highly glycolytic, have mutated p53 sequences (exon 8, codon 273 and exon 5, codon 135, respectively), while IGROV-1 and PDOVCA#4 cells, which are poorly glycolytic, have wild-type p53 alleles. This observation, albeit correlative, may indicate that the p53 status could contribute to the determination of the metabolic profile of ovarian cancer cells. Alternatively, the metabolic differences detected could be sustained by different ATP turnover rates in OC316 and IGROV-1 cells. Hypothetically, if OC316 cells had a faster metabolic rate than IGROV-1 cells, they might require more rapid ATP production via both glycolysis and oxidative phosphorylation. Although not supported by measurements of ATP steady-state levels and the decline in ATP levels following substrate deprivation (Figure 1E), we cannot completely rule out this possibility, as ATP synthesis from endogenous substrates might have affected our measurements to some extend.

Highly glycolytic ovarian cancer cells disclosed the highest levels of hypoxia-induced cell death (Figure 2). Dead cells presented some phenotypic features of late apoptosis/necrosis, as previously observed in malignant glioma cells.[18] Reduction of time of incubation under hypoxic conditions to 24 hours decreased the percentage of dead cells, yet they remained essentially Annexin V^+/PI^+ (not shown). Moreover, cell death was found to occur when glucose availability became limited and cellular ATP was progressively depleted. Altogether, these results fit the hypothesis that glucose becomes a critical substrate for the maintenance of the intracellular ATP levels under hypoxic conditions and, in fact, supplementation of glucose to the culture medium protected cancer cells from hypoxia-induced cell death, in agreement with findings previously obtained with normal cell types[39–41] and tumor cells.[18]

If this hypothesis is correct, why did attenuation of HIF-1α expression further increase tumor cell death?

Indeed, since HIF-1α is known to enhance glycolysis, OC316 ΔHIF-1α cells were expected to have reduced glucose consumption. In our model, however, expression of the HIF-1α-dependent glycolysis-associated genes as well as lactic acid production were only slightly reduced in OC316 ΔHIF-1α compared to control cells (Supplementary Figure S2 at *http://ajp.amjpathol.org*), which indicates that other pathways may control glycolysis in presence of HIF-1α knockdown. The unexpected finding that OC316 ΔHIF-1α tumors had relatively high and similar lactate concentrations as control tumors according to metabolic imaging (Figure 8), also reinforces the evidence that HIF inactivation did not significantly impair the glycolytic capacity of these cells.

Recently it was found that pyruvate dehydrogenase kinase 1 is a HIF-1 target gene that influences mitochondrial function by limiting pyruvate entry into the tricarboxylic acid cycle and thus suppressing both the tricarboxylic acid cycle and respiration.[42,43] Although we did not address this in our study, it is possible that increased death of HIF-1-deficient cells could be partly due to reduced pyruvate dehydrogenase kinase 1 levels and lack of mitochondrial shut-down under severe hypoxia, thus leading to reactive oxygen species-mediated cell damage.

Based on our data, however, the most likely explanation for the increased hypoxic death of HIF-1-deficient tumor cells stems from the prominent effects of HIF-1α silencing on cell proliferation and, consequently, on the metabolic rate of the tumor cells. Under hypoxic conditions, indeed, proliferation of OC316 ΔHIF-1α cells did not slow down (Figure 5) and this was associated with differences in the phosphorylation levels of Rb as well as increased c-Myc activity compared to controls, thus confirming previous studies on the regulation of cell proliferation by HIF-1.[27,30] The sustained nutrient demand eventually caused anticipated exhaustion of ATP and acceleration of cell death. These data reinforce the evidence that HIF-1α in certain contexts is a potent inhibitor of cell proliferation.[44–47] Since OC316 cells express also HIF-2α (not shown), which is emerging as a positive regulator of cell proliferation under hypoxic conditions, as opposed to HIF-1α,[31] it could be that HIF-1α silencing introduces an unbalance between these two factors which favors cell proliferation by a c-Myc-mediated mechanism. Moreover, increased proliferation could conceivably account for the very low ATP levels and the increased areas of necrosis in tumors formed by HIF-1α-deficient cells.

In the last part of the study, we investigated the effects of modulation of HIF-1α on tumor formation. Previous studies on this matter have reported conflicting results. Some laboratories have indeed demonstrated that loss of HIF-1α delays tumor growth,[48–53] usually through angiogenesis and/or glycolysis inhibition. Other studies, however, come to opposite conclusions describing HIF-1α as a tumor suppressor gene, possibly through its interaction with p53 or c-myc under hypoxic conditions.[28,45]

In our system HIF-1α inactivation increased cell death, but it did not significantly reduce tumor growth in two different locations. One possible explanation for this was a reduced angiogenic capacity of tumor cells lacking HIF-1α, due to down-regulation of VEGF expression. Vascularization, however, was not appreciably compromised, possibly due to functional compensation of diminished VEGF levels through other angiogenic factors, which are abundantly expressed by OC316 ΔHIF-1α cells (Figure 7). Moreover, the abundant areas of necrosis in OC316 ΔHIF-1α tumors recruited many F4/80+ macrophages (data not shown) that could compensate, by releasing murine angiogenic factors, the reduced production of human VEGF by the tumor cells. In any case, maintenance of the angiogenic phenotype in tumor cells lacking HIF-1α has also been reported in other studies.[48,51,52]

It is also worth noting that the results presented here could have therapeutic implications. Ovarian cancer remains the most lethal of gynecologic malignancies with dismal long-term survival rates,[54] thus demanding the development of novel therapies.

Several anti-HIF drugs are under development, and they have shown encouraging results in pre-clinical models (reviewed in:[55]). Hypothetically, therapeutic effects of these drugs could in part depend on the proliferation rate and the metabolic profile of tumor cells, two clinically measurable parameters. Moreover, as HIF attenuation appears to boost cell proliferation and thus increase glucose demand by the tumor, it could be convenient to combine HIF-specific drugs with anti-angiogenic therapy, which limits oxygen and nutrients supply. In conclusion, our findings underscore the need for further studies oriented at determining whether HIF inactivation conveys sensitivity to anti-angiogenic treatments.

Acknowledgments

We thank Esther Wenzel, Enrica Cannizzaro, and Ilaria Ricci for technical assistance, Prof. Francesco Lisi (Department of Statistics, University of Padova, Padova, Italy) for statistical analysis, Ms. Colette Case for editing the manuscript and Prof. Adrian L. Harris (Weatherall Institute of Molecular Medicine, Oxford, UK) and Prof. Antonella Naldini (University of Siena, Siena, Italy) for critical reading of the manuscript. We are grateful to Dr. S. Ferrini (Istituto Nazionale per la Ricerca sul Cancro, Genoa, Italy), Dr. O.V. Razorenova (Department of Molecular Cardiology, Lerner Research Institute, Cleveland, OH), Dr. S. Pennacchietti (Istituto per la Ricerca e la Cura del Cancro, Candiolo, Torino, Italy), and Prof. Celeste M. Simon (Department of Cell and Developmental Biology, Abramson Cancer Research Institute, Philadelphia, PA) for providing reagents used in this study.

References

1. Harris AL: Hypoxia–a key regulatory factor in tumour growth. Nat Rev Cancer 2002, 2:38–47
2. Fenton BM, Paoni SF, Ding I: Effect of VEGF receptor-2 antibody on vascular function and oxygenation in spontaneous and transplanted tumors. Radiother Oncol 2004, 72:221–230
3. Franco M, Man S, Chen L, Emmenegger U, Shaked Y, Cheung AM, Brown AS, Hicklin DJ, Foster FS, Kerbel RS: Targeted anti-vascular endothelial growth factor receptor-2 therapy leads to short-term and long-term impairment of vascular function and increase in tumor hypoxia. Cancer Res 2006, 66:3639–3648
4. Winkler F, Kozin SV, Tong RT, Chae SS, Booth MF, Garkavtsev I, Xu L, Hicklin DJ, Fukumura D, di Tomaso E, Munn LL, Jain RK: Kinetics of vascular normalization by VEGFR2 blockade governs brain tumor response to radiation: role of oxygenation, angiopoietin-1, and matrix metalloproteinases. Cancer Cell 2004, 6:553–563
5. Ferrara N, Kerbel RS: Angiogenesis as a therapeutic target. Nature 2005, 438:967–974
6. Semenza GL: Targeting HIF-1 for cancer therapy. Nat Rev Cancer 2003, 3:721–732
7. Bacon AL, Harris AL: Hypoxia-inducible factors and hypoxic cell death in tumour physiology. Ann Med 2004, 36:530–539
8. Pouyssegur J, Dayan F, Mazure NM: Hypoxia signalling in cancer and approaches to enforce tumour regression. Nature 2006, 441:437–443

9. Gatenby RA, Gillies RJ: Why do cancers have high aerobic glycolysis? Nat Rev Cancer 2004, 4:891–899
10. Warburg O: On respiratory impairment in cancer cells. Science 1956, 124:269–270
11. Bos R, van Der Hoeven JJ, van Der Wall E, van Der Groep P, van Diest PJ, Comans EF, Joshi U, Semenza GL, Hoekstra OS, Lammertsma AA, Molthoff CF: Biologic correlates of (18)fluorodeoxyglucose uptake in human breast cancer measured by positron emission tomography. J Clin Oncol 2002, 20:379–387
12. Papandreou I, Krishna C, Kaper F, Cai D, Giaccia AJ, Denko NC: Anoxia is necessary for tumor cell toxicity caused by a low-oxygen environment. Cancer Res 2005, 65:3171–3178
13. Amellem O, Stokke T, Sandvik JA, Smedshammer L, Pettersen EO: Hypoxia-induced apoptosis in human cells with normal p53 status and function, without any alteration in the nuclear protein level. Exp Cell Res 1997, 232:361–370
14. Araya R, Uehara T, Nomura Y: Hypoxia induces apoptosis in human neuroblastoma SK-N-MC cells by caspase activation accompanying cytochrome c release from mitochondria. FEBS Lett 1998, 439:168–172
15. Brunelle JK, Santore MT, Budinger GR, Tang Y, Barrett TA, Zong WX, Kandel E, Keith B, Simon MC, Thompson CB, Hay N, Chandel NS: c-Myc sensitization to oxygen deprivation-induced cell death is dependent on Bax/Bak, but is independent of p53 and hypoxia-inducible factor-1. J Biol Chem 2004, 279:4305–4312
16. Graeber TG, Osmanian C, Jacks T, Housman DE, Koch CJ, Lowe SW, Giaccia AJ: Hypoxia-mediated selection of cells with diminished apoptotic potential in solid tumours. Nature 1996, 379:88–91
17. Hockel M, Schlenger K, Hockel S, Vaupel P: Hypoxic cervical cancers with low apoptotic index are highly aggressive. Cancer Res 1999, 59:4525–4528
18. Steinbach JP, Wolburg H, Klumpp A, Probst H, Weller M: Hypoxia-induced cell death in human malignant glioma cells: energy deprivation promotes decoupling of mitochondrial cytochrome c release from caspase processing and necrotic cell death. Cell Death Differ 2003, 10:823–832
19. Yao KS, Clayton M, O'Dwyer PJ: Apoptosis in human adenocarcinoma HT29 cells induced by exposure to hypoxia. J Natl Cancer Inst 1995, 87:117–122
20. Indraccolo S, Tisato V, Agata S, Moserle L, Ferrari S, Callegaro M, Persano L, Palma MD, Scaini MC, Esposito G, Fassina A, Nicoletto O, Plebani M, Chieco-Bianchi L, Amadori A, D'Andrea E, Montagna M: Establishment and characterization of xenografts and cancer cell cultures derived from BRCA1−/− epithelial ovarian cancers. Eur J Cancer 2006, 42:1475–1483
21. Razorenova OV, Ivanov AV, Budanov AV, Chumakov PM: Virus-based reporter systems for monitoring transcriptional activity of hypoxia-inducible factor 1. Gene 2005, 350:89–98
22. Indraccolo S, Habeler W, Tisato V, Stievano L, Piovan E, Tosello V, Esposito G, Wagner R, Uberla K, Chieco-Bianchi L, Amadori A: Gene transfer in ovarian cancer cells: a comparison between retroviral and lentiviral vectors. Cancer Res 2002, 62:6099–6107
23. Indraccolo S, Tisato V, Tosello V, Habeler W, Esposito G, Moserle L, Stievano L, Persano L, Chieco-Bianchi L, Amadori A: Interferon-alpha gene therapy by lentiviral vectors contrasts ovarian cancer growth through angiogenesis inhibition. Hum Gene Ther 2005, 16:957–970
24. Indraccolo S, Stievano L, Minuzzo S, Tosello V, Esposito G, Piovan E, Zamarchi R, Chieco-Bianchi L, Amadori A: Interruption of tumor dormancy by a transient angiogenic burst within the tumor microenvironment. Proc Natl Acad Sci USA 2006, 103:4216–4221
25. Walenta S, Schroeder T, Mueller-Klieser W: Metabolic mapping with bioluminescence: basic and clinical relevance. Biomol Eng 2002, 18:249–262
26. Walenta S, Schroeder T, Mueller-Klieser W: Lactate in solid malignant tumors: potential basis of a metabolic classification in clinical oncology. Curr Med Chem 2004, 11:2195–2204
27. Goda N, Ryan HE, Khadivi B, McNulty W, Rickert RC, Johnson RS: Hypoxia-inducible factor 1alpha is essential for cell cycle arrest during hypoxia. Mol Cell Biol 2003, 23:359–369
28. Koshiji M, Huang LE: Dynamic balancing of the dual nature of HIF-1alpha for cell survival. Cell Cycle 2004, 3:853–854
29. Wang G, Reisdorph R, Clark RE Jr, Miskimins R, Lindahl R, Miskimins WK: Cyclin dependent kinase inhibitor p27(Kip1) is up-regulated by hypoxia via an ARNT dependent pathway. J Cell Biochem 2003, 90:548–560
30. Koshiji M, Kageyama Y, Pete EA, Horikawa I, Barrett JC, Huang LE: HIF-1alpha induces cell cycle arrest by functionally counteracting Myc. EMBO J 2004, 23:1949–1956
31. Gordan JD, Bertout JA, Hu CJ, Diehl JA, Simon MC: HIF-2alpha promotes hypoxic cell proliferation by enhancing c-myc transcriptional activity. Cancer Cell 2007, 11:335–347
32. Quennet V, Yaromina A, Zips D, Rosner A, Walenta S, Baumann M, Mueller-Klieser W: Tumor lactate content predicts for response to fractionated irradiation of human squamous cell carcinomas in nude mice. Radiother Oncol 2006, 81:130–135
33. Greijer AE, van der Wall E: The role of hypoxia inducible factor 1 (HIF-1) in hypoxia induced apoptosis. J Clin Pathol 2004, 57:1009–1014
34. Piret JP, Mottet D, Raes M, Michiels C: Is HIF-1alpha a pro- or an anti-apoptotic protein? Biochem Pharmacol 2002, 64:889–892
35. Nakayama K, Kanzaki A, Hata K, Katabuchi H, Okamura H, Miyazaki K, Fukumoto M, Takebayashi Y: Hypoxia-inducible factor 1 alpha (HIF-1 alpha) gene expression in human ovarian carcinoma. Cancer Lett 2002, 176:215–223
36. Birner P, Schindl M, Obermair A, Breitenecker G, Oberhuber G: Expression of hypoxia-inducible factor 1alpha in epithelial ovarian tumors: its impact on prognosis and on response to chemotherapy. Clin Cancer Res 2001, 7:1661–1668
37. Zhong H, De Marzo AM, Laughner E, Lim M, Hilton DA, Zagzag D, Buechler P, Isaacs WB, Semenza GL, Simons JW: Overexpression of hypoxia-inducible factor 1alpha in common human cancers and their metastases. Cancer Res 1999, 59:5830–5835
38. Matoba S, Kang JG, Patino WD, Wragg A, Boehm M, Gavrilova O, Hurley PJ, Bunz F, Hwang PM: p53 regulates mitochondrial respiration. Science 2006, 312:1650–1653
39. Callahan DJ, Engle MJ, Volpe JJ: Hypoxic injury to developing glial cells: protective effect of high glucose. Pediatr Res 1990, 27:186–190
40. Saikumar P, Dong Z, Patel Y, Hall K, Hopfer U, Weinberg JM, Venkatachalam MA: Role of hypoxia-induced Bax translocation and cytochrome c release in reoxygenation injury. Oncogene 1998, 17:3401–3415
41. Malhotra R, Brosius FC, 3rd: Glucose uptake and glycolysis reduce hypoxia-induced apoptosis in cultured neonatal rat cardiac myocytes. J Biol Chem 1999, 274:12567–12575
42. Kim JW, Tchernyshyov I, Semenza GL, Dang CV: HIF-1-mediated expression of pyruvate dehydrogenase kinase: a metabolic switch required for cellular adaptation to hypoxia. Cell Metab 2006, 3:177–185
43. Papandreou I, Cairns RA, Fontana L, Lim AL, Denko NC: HIF-1 mediates adaptation to hypoxia by actively down-regulating mitochondrial oxygen consumption. Cell Metab 2006, 3:187–197
44. Blouw B, Song H, Tihan T, Bosze J, Ferrara N, Gerber HP, Johnson RS, Bergers G: The hypoxic response of tumors is dependent on their microenvironment. Cancer Cell 2003, 4:133–146
45. Carmeliet P, Dor Y, Herbert JM, Fukumura D, Brusselmans K, Dewerchin M, Neeman M, Bono F, Abramovitch R, Maxwell P, Koch CJ, Ratcliffe P, Moons L, Jain RK, Collen D, Keshert E: Role of HIF-1alpha in hypoxia-mediated apoptosis, cell proliferation and tumour angiogenesis. Nature 1998, 394:485–490
46. Leek RD, Stratford I, Harris AL: The role of hypoxia-inducible factor-1 in three-dimensional tumor growth, apoptosis, and regulation by the insulin-signaling pathway. Cancer Res 2005, 65:4147–4152
47. Mack FA, Rathmell WK, Arsham AM, Gnarra J, Keith B, Simon MC: Loss of pVHL is sufficient to cause HIF dysregulation in primary cells but does not promote tumor growth. Cancer Cell 2003, 3:75–88
48. Chen J, Zhao S, Nakada K, Kuge Y, Tamaki N, Okada F, Wang J, Shindo M, Higashino F, Takeda K, Asaka M, Katoh H, Sugiyama T, Hosokawa M, Kobayashi M: Dominant-negative hypoxia-inducible factor-1 alpha reduces tumorigenicity of pancreatic cancer cells through the suppression of glucose metabolism. Am J Pathol 2003, 162:1283–1291
49. Li J, Shi M, Cao Y, Yuan W, Pang T, Li B, Sun Z, Chen L, Zhao RC: Knockdown of hypoxia-inducible factor-1alpha in breast carcinoma MCF-7 cells results in reduced tumor growth and increased sensitivity to methotrexate. Biochem Biophys Res Commun 2006, 342:1341–1351

50. Li L, Lin X, Staver M, Shoemaker A, Semizarov D, Fesik SW, Shen Y: Evaluating hypoxia-inducible factor-1alpha as a cancer therapeutic target via inducible RNA interference in vivo. Cancer Res 2005, 65:7249–7258
51. Mizukami Y, Jo WS, Duerr EM, Gala M, Li J, Zhang X, Zimmer MA, Iliopoulos O, Zukerberg LR, Kohgo Y, Lynch MP, Rueda BR, Chung DC: Induction of interleukin-8 preserves the angiogenic response in HIF-1alpha-deficient colon cancer cells. Nat Med 2005, 11:992–997
52. Ryan HE, Poloni M, McNulty W, Elson D, Gassmann M, Arbeit JM, Johnson RS: Hypoxia-inducible factor-1alpha is a positive factor in solid tumor growth. Cancer Res 2000, 60:4010–4015
53. Stoeltzing O, McCarty MF, Wey JS, Fan F, Liu W, Belcheva A, Bucana CD, Semenza GL, Ellis LM: Role of hypoxia-inducible factor 1alpha in gastric cancer cell growth, angiogenesis, and vessel maturation. J Natl Cancer Inst 2004, 96:946–956
54. Burger RA: Experience with bevacizumab in the management of epithelial ovarian cancer. J Clin Oncol 2007, 25:2902–2908
55. Melillo G: Inhibiting hypoxia-inducible factor 1 for cancer therapy. Mol Cancer Res 2006, 4:601–605